LAWRENCE
LIVERMORE
NATIONAL
LABORATORY

LLNL-JRNL-410658

Observations of electromagnetic fields and plasma flow in hohlraums with proton radiography

C. K. Li, F. H. Seguin, J. A. Frenje, R. D. Petrasso, P. A. Amendt, R. P. J. Town, O. L. Landen, J. R. Rygg, R. Betti, J. P. Knauer, D. D. Meyerhofer, J. M. Soures, C. A. Back, J. D. Kilkenny, A. Nikroo

February 18, 2009

Physical Review Letters

Disclaimer

Observations of electromagnetic fields and plasma flow in hohlraums with proton radiography

C. K. Li, F. H. Séguin, J. A. Frenje, and R. D. Petrasso
Plasma Science and Fusion Center, Massachusetts Institute of Technology, Cambridge, Massachusetts 02139, USA

P. A. Amendt, R. P. J. Town, O. L. Landen, and J. R. Rygg
Lawrence Livermore National Laboratory, Livermore, California 94550 USA

R. Betti*, J. P. Knauer, D. D. Meyerhofer*, and J. M. Soures
Laboratory for Laser Energetics, University of Rochester, Rochester, New York 14623, USA

C. A. Back, J. D. Kilkenny, and A. Nikroo
General Atomics, San Diego, California, 92186 USA

We report on the first proton radiography of laser-irradiated hohlraums. This experiment, with vacuum gold (Au) hohlraums, resulted in observations of self-generated electric and magnetic fields. Peak values are ~ 10^9 V m^{-1} and ~ 10^6 gauss. Time-gated radiographs of monoenergetic protons with discrete energies (15.0 and 3.3 MeV) reveal dynamic pictures of field structures and plasma flow. Near the end of the 1-ns laser drive, a stagnating Au plasma (~ 10 mg cm^{-3}) forms at the center of the hohlraum, a consequence of supersonic, radially directed Au jets (~ 1000 μm ns^{-1}, ~ Mach 4) as laser-driven plasma bubbles approaching one another.

PACS numbers: 52.38.Fz, 52.30.-q, 52.57.-z, 52.50.Jm

A high-Z enclosure, *i.e.* hohlraum, creates an environment filled with a nearly blackbody (Planckian) radiation field when irradiated by high-power lasers or energetic ions [1,2]. The cavity generates intense thermal x rays at a radiation temperature (T_r) of hundreds of eV. Hohlraums have been extensively used as radiation sources or platforms for a wide range of basic and applied physics experiments. In studies of laboratory astrophysics and high-energy-density (HED) physics [3,4], for example, hohlraums are used for creating and simulating various extreme HED conditions, including those of stellar and planetary interiors. The hohlraum radiation field is used to compress spherical capsules, through capsule ablation, to high temperature and density in indirect-drive inertial-confinement fusion (ICF) [1,2].

The use of hohlraums requires an understanding of physics details, such as coupling efficiency, plasma conditions, instabilities, radiation uniformity [1,2,5,6] and cavity shape [1,2,7,8]. Electric (E) and magnetic (B) fields generated by several processes may have important effects on hohlraum physics and overall performance [9-11]. For example, B fields inside a hohlraum can reduce heat flow, since cross-field thermal conductivity is modified by a factor of $(1+\omega_{ce}^2\tau^2)^{-1}$, where ω_{ce} is the electron gyro frequency and τ is the collision time [12,13]. E fields may modify the plasma distribution and conditions and, if sufficiently large, could potentially enhance thick-target bremsstrahlung at x-ray energies well above the Planckian background [14]. Thus such fields could alter distributions of electron temperature (T_e) and density (n_e), affecting laser-plasma instabilities and drive uniformity.

For low-intensity laser drive, such as characterized by most hohlraum experiments [1-11], the dominant source for B-field generation is expected to be non-parallel electron density and temperature gradients ($\nabla n_e \times \nabla T_e$) [12,13]. The E field is expected to result from electron pressure gradients (∇P_e) [12,13]. Despite such expectations, prior to this work, no direct experimental measurement and characterization of such hohlraum fields have been made.

The first observations of E and B fields, and their evolution in hohlraums, are presented in this Letter. Coupled plasma flow dynamics were also observed. The technique used was time-gated radiography with monoenergetic 3.3- and 15-MeV protons [15]. Simultaneous imaging with two discrete proton energies breaks any inherent degeneracy between E and B. These measurements directly reveal new physical phenomena and provide a previously unavailable, stringent test for developing and validating 3-dimensional (3D) radiation-hydrodynamic and kinetic codes [16].

The experiments, illustrated schematically in Fig. 1, were performed at the OMEGA laser facility [17]. The proton sources were D^3He-filled, thin-glass-shell targets driven by 21 OMEGA laser beams, each producing a ~ 130-ps-long pulse of protons; the relative timing of backlighter and subject hohlraum drive was adjusted [15] to sample the hohlraum at a desired time. The proton radiographs were recorded using CR-39 detectors [18], and the isotropy of the backlighter allows two different experiments to be performed simultaneously in each shot (Fig. 1a). The hohlraums were of the OMEGA scale-1.5 size [1] with 30-μm-thick gold walls, 100% laser-entrance holes (LEH), 2.4-mm diameter, and 2-mm length. Each hohlraum was driven by 10 laser beams (incident angle 58.8°) forming a single irradiation ring with total laser energy ~ 4 kJ in a 1-ns square pulse. The individual laser beams had full spatial and temporal smoothing [19]. SG4 phase plates resulted in each beam illuminating an elliptical spot on the wall with a ratio of long-to-short axis ~ 1.2 and laser intensity ~ 2×10^{14} W cm^{-2}. A nickel mesh (60 μm thick, 150-μm hole-to-hole spacing, and 75-μm square holes) [15] was used to divide

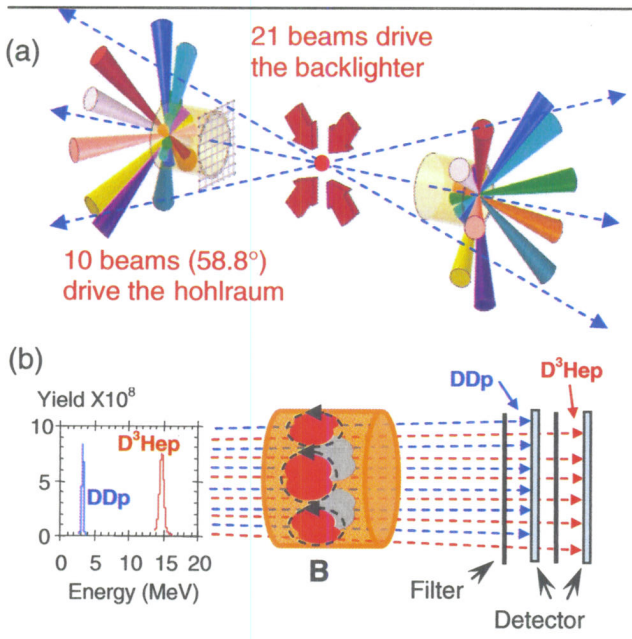

FIG. 1. (Color) Experimental setup (a), with proton backlighter, subject hohlraums, and laser beams. The distance between the backlighter and the mesh (detector) was 0.7 (27) cm. Typical energy spectrum and "sandwich-like" detector are shown in (b). The filters and the thickness of the front detector were carefully chosen so that 3.3-MeV DD protons were recorded only on that detector while 15-MeV D^3He protons were recorded only on the second detector [18].

backlighter protons into discrete beamlets to allow quantitative measurement of proton trajectory displacements due to fields.

Figure 2 shows sequences of proton images obtained on five different shots, covering a time period from the beginning of the laser pulse ($t = 0$ ns) to 0.8 ns after it was off ($t \approx 1.8$ ns). At earlier times ($t \leq 0.9$ ns) the 15-MeV images (Fig. 2a) have arrays of beamlets showing minimal displacement by fields or plasma, but individual beamlets have different sizes, reflecting more subtle field effects; at late times the 15-MeV beamlets show some chaotic spatial structure, indicating that their trajectories have been affected by large field and plasma effects (such an erratic pattern may help to explain the asymmetries of self-emitted 15-MeV proton fluxes from an indirect-drive capsule implosion [10]). In the 3.3-MeV images (Fig. 2b), the arrays of proton beamlets are coherently distorted by the time t = 0.52 ns, and the individual beamlets disappear due to stronger deflections at later times.

Angular deflection of each beamlet is proportional to both $\int \mathbf{B} \times d\ell$ and $\int \mathbf{E} \times d\ell$ (where $d\ell$ is the differential pathlength along the proton trajectory). For certain situations with enough symmetry, the potential degeneracy between E and B can be broken [20,21]. Here this is overcome by near-simultaneous 3.3 and 15 MeV radiographs. Because of the Lorentz force, deflections due to B are inversely proportional to the square root of proton energy ($\xi \propto \varepsilon_p^{-1/2}$) while those due to E are inversely proportional to proton energy ($\xi \propto \varepsilon_p^{-1}$). Thus measuring beamlet displacements in images from a single shot with these distinct proton energies (ignoring small flight time differences) breaks the degeneracy.

The lineouts in Fig. 3 show that the arrays of beamlets are approximately uniformly spaced in the hohlraum center region for both 15-MeV (Fig. 3a) and 3.3-MeV protons (Fig. 3b), but that they expand, by different amounts in the proximity of the hohlraum wall. The displacements are estimated to be ≈ 30 μm for 15-MeV protons and ≈ 75 μm for 3.3-MeV protons. These displacements have a ratio 75/30 ~ 2.5, which is close to the square root of the energy ratio $(15/3.3)^{1/2} \approx 2.2$ expected from B-field deflection, but far from the energy ratio (15/3.3) ≈ 4.6 expected from E-field deflections. This comparison suggests that the B field is the dominant source for the observed proton deflections.

Estimating the absolute magnitude of B field requires consideration of the proton trajectories near the hohlraum wall, where they encounter two regions of B field with opposing signs as they pass through the two sides of the plasma bubble produced by a laser-wall interaction [15]). The deflections occurring in the two regions do not exactly cancel because the trajectories of protons are not exactly parallel to the axis of the hohlraum (2D LASNEX radiation-hydrodynamic simulations [22] indicate a ~ 10% asymmetry in opposing displacements). Using either $\xi \sim 30$ or 75 μm and $\delta B \propto \xi \varepsilon_p^{1/2} L_B^{-1}$ [15], where $L_B \sim L_T \equiv T_e (\nabla T_e)^{-1}$ is the temperature scale length which is about the radius of the plasma bubble (~ 200 - 400 μm) [15], the net δB is ~ 0.1×10^6 gauss (about half that predicted by LASNEX). Taking the cancellation asymmetry factor to be 10 implies a maximum B field of ~ 1×10^6 gauss (MG).

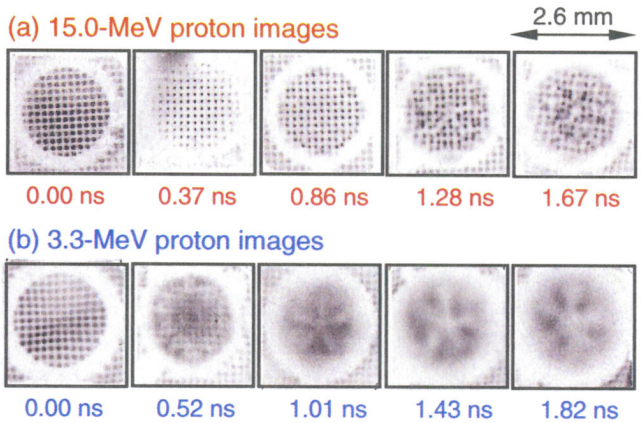

FIG. 2. (Color online) Radiographs of a 10-laser-beam driven Au hohlraum at different times, taken with 15.0-MeV D^3He protons (a), and 3.3-MeV DD protons (b), illustrating spatial structure and time evolution of proton deflection and beamlet size (within each image, darker means higher fluence). The corresponding pairs of the images in (a) and (b) were taken in the same shot, but give different sample times due to different proton velocities. The gray-scale mapping of the image display is different in each image to account for the different backlighter yields and to make the most important structures clearly visible.

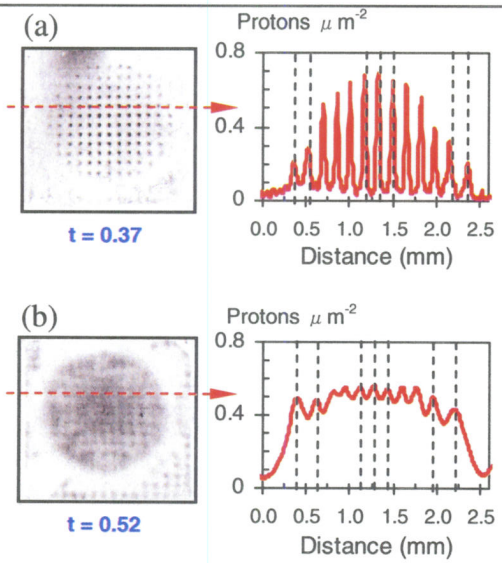

FIG. 3. (Color online) Lineouts indicate that the arrays of beamlets are slightly expanded in proximity to the hohlraum wall; displacements $\xi \sim 30$ μm and ~ 75 μm for 15-MeV (a) and 3.3-MeV (b) protons, respectively.

Electrical charging of the hohlraum, which is electrically connected to the Ni grid, is indicated by the apparent hole-size reduction seen most clearly in the 15 MeV radiograph at 0.37 ns and the lineout plotted in Fig. 4a (symmetry requires that this apparent constriction is an *E*-field effect). The *E*-field associated with this constriction can be estimated from a simple formula based on the experimental geometry: $E \approx 4\varepsilon_p q^{-1} L_E^{-2} \Delta$, where $\Delta \approx 0.5A(D-\varpi)L_E a^{-1}(A-a+L_E)^{-1}$ is the apparent displacement at the mesh plane; D is the grid hole spacing (75 μm); ϖ is the width (FWHM) of the lineout at the mesh plane; a (A) is the distance from backlighter to mesh (detector); q is the proton charge; and L_E is the field scale length. Protons see a transverse field mainly as they enter a mesh hole, and the scale length along their trajectory is about the transverse size of the hole, or 75 μm. The field estimates for different times are plotted in Fig. 4b, showing that a peak E field ~ 2×10^9 V m^{-1} occurs at ~ 0.37 ns. For this mm-scale size hohlraum, such a peak field would indicate peak charging to ~ 10^6 volts (MV). Interestingly, the field is seen to decay away, a likely consequence of discharging, even while the laser drives on (Fig 4b). Similar charging and discharging effects have been seen for (arbitrary) targets irradiated by lasers of this intensity. It is this effect that, for thin-glass-shell targets of the experiments herein and elsewhere [23], causes the slight upshift in the nuclear fusion birth energy from 3.0 (14.7) MeV to 3.3 (15.0) MeV.

A striking feature in Fig. 2 is a 5-prong asterisk-like fluence pattern in the DD proton images at $t \geq 1.01$ ns and later [24]. As illustrated in Fig. 5, such an asterisk is a direct consequence of the staggered distribution of laser beams on the hohlraum wall. Although all incident at 58.8° to the normal, the ten laser beams are grouped to form five pairs with 26.8° between two beams within

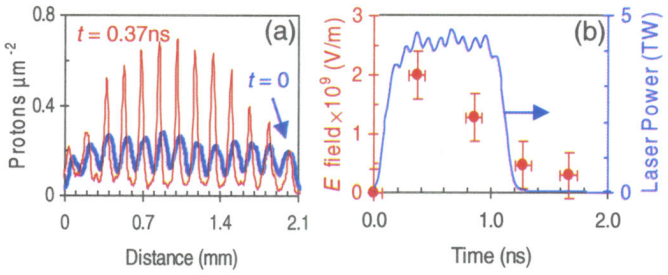

FIG. 4 (Color) (a) Lineouts from 15-MeV images of t = 0.0 and 0.37 ns, shown in Fig. 2a. The characteristic widths ϖ (FWHM) are the measure of the beamlets on the mesh plane. (b) E fields estimated from experimental measurements (solid circles).

each pair, but 45.2° between adjacent pairs (Fig. 5a). For the experimental conditions (T_e ~ 1 keV, T_i ~ 1 eV, and n_e ~ $0.1n_c$), the plasmas have high β ($\equiv 8\pi n_e k T_e B^{-2}$ ~ 10-100) and a sound speed [$C_s \sim (ZT_e m_i^{-1})^{1/2}$ ~ 200 - 300 μm ns^{-1}] that sets a scale for hydrodynamic expansion. With ~ 200 μm between pairs of bubbles (Fig. 5a), it is expected that adjacent approaching bubbles should coalesce in ~ 0.35 ns and move inward toward the hohlraum axis in ~ 3 - 4 ns. In contrast the 3.3 MeV radiograph at 1.01 ns indicates, on the basis of the 5-prong asterisk pattern, that Au-plasma jets shoot inward at about ~ Mach 4 (~ 1000 μm ns^{-1}). The subsequent 3.3-MeV radiograph at 1.43 ns shows a much more enhanced asterisk pattern. A faint outline of the same asterisk pattern is shown on the corresponding 15-MeV radiograph (at 1.28 ns). From this latter set of radiographs (Fig. 5c), the size of the proton-fluence depletion region in a leg of the asterisk is ~ 50 (260) μm for the 15 (3.3) MeV protons. If depletion is a

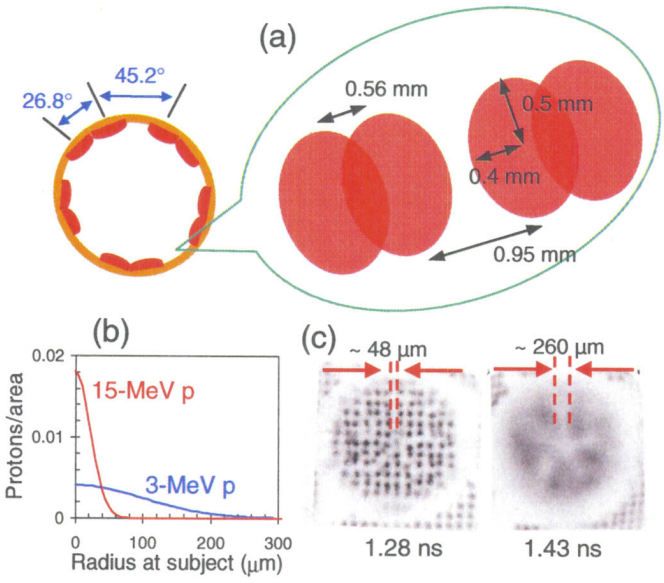

FIG.5. (Color online) Carton to illustrate laser beam distribution in OMEGA Cone 3 configuration (a). Calculated proton scattering distributions at subject plane for a ~ 1 mg cm^{-2} Au plasma (b) It is shown that, the scattering width (FWMH) for 3-MeV protons is 235 μm, while scattering width (FWMH) for 15-MeV protons is 52 μm. These estimates are comparable with the measured widths (c) of the stagnating plasma (~ 260 μm and ~ 48 μm, respectively).

result of scattering off the Au plasma, its density can be estimated. Figure 5b shows the effects of scattering calculated for 3.3 and 15 MeV protons in a 1 mg cm^{-2} Au plasma [25]. As the scattering width goes inversely with the proton energy [26], the 3.3 MeV scattering profile is broader by about a factor 5. The observations (Fig 5c) for both the 3.3 and 15 MeV protons are thus consistent with 1 mg cm^{-2} Au [27]. Taking the scale size for the Au plasma (in the direction of the hohlraum axis) to be ~1 mm, the Au density is ~ 10 mg cm^{-3}.

To explore aspects of these 3D phenomena, highly resolved 1D LASNEX hydrodynamic simulations were run with the Au-plasma bubble expanding into an ultra-low density vacuum. These initial simulations indicate an expansion rate comparable to the jets. However, in addition to this pure hydrodynamic expansion, an added kinetic effect from the hot electrons advancing ahead of the rarefaction expansion will further boost the motion of the Au ions by the ion sound speed [28]. Work is in progress to assess whether such a hybrid motion of the Au bubble is sufficient to generate the ~10 mg cm^{-3} stagnation density on the symmetry axis by ~1 ns.

In summary, we report on the first observations of *E* and *B* fields associated with laser-irradiated hohlraums. Time-gated radiographs of monoenergetic protons with discrete energies (15.0 and 3.3 MeV) reveal a dynamic picture of field structure during and after the laser drive. Discrete but disparate monoenergetic proton energies enable discrimination between *E* and *B* fields. Peak fields were ~ 10^9 V m^{-1} and ~ 10^6 gauss. An Au plasma (~ 10 mg cm^{-3}) stagnates on the hohlraum axis by 1 ns due to ~ Mach 4 (v ~1000 μm ns^{-1}) jets that form between adjacent laser-generated plasma bubbles (note that this should not occur in an ignition hohlraum, where gas fill would impede the jets). These experimental results have important implications for understanding the precise conditions and plasma dynamics inside vacuum hohlraums and provide an impetus for the further development of 3D multi-fluid codes with self-consistent field generation.

The authors thank Dr. L. J. Suter and Dr. S. H. Glenzer of LLNL for useful discussions. The work was performed at the LLE National Laser User's Facility (NLUF), and was supported in part by US DOE (DE-FG52-07NA28059 and DE-FG52-06N826203), LLNL (B543881), LLE (414090-G), the Fusion Science Center at University of Rochester (412761-G), and GA (DE-AC52-06NA27279). Prepared by LLNL under Contract DE-AC52-07NA27344.

* Also at Department of Mechanical Engineering, and Physics and Astronomy, University of Rochester.

[1] J. D. Lindl, *Inertial Confinement Fusion* (Springer-Verlag, New York 1999).
[2] S. Atzeni and J. Meyer-Ter-Vehn, *The Physics of Inertial Fusion* (Clarendon Press, Oxford 2004).
[3] R. P. Drake, *High-Energy-Density Physics* (Springer Press, New York, 2006).
[4] B. A. Remington *et al.*, Science **284**, 1488 (1999).
[5] L. J. Suter Phys. Rev. Lett. **73**, 2328 (1995).
[6] M. D. Rosen *et al.*, Phys. Rev. E **72**, 056403 (2005).
[7] M. Vandenboomgaerde *et al.*, Phys. Rev. Lett. **99**, 065004 (2007).
[8] P. A. Amendt *et al.*, Phys. Plasmas 15, 012702 (2008).
[9] S. H. Glenzer *et al.*, Phys. Rev. Lett. **87**, 045002 (2001).
[10]P. A. Amendt *et al.*, Bull. Am. Phys. Soc. **49**, 26 (2004).
[11] R. P. J. Town *et al.*, Bull.Am.Phys. Soc. **50**, 123 (2005).
[12] S. I. Braginskii, *Review of Plasma Physics 1* (Consultants Bureau, New York, 1965).
[13] M. G. Haines, Phys. Rev. Lett. **78**, 254 (1997).
[14]M. B. Schneider *et al.*, Phys. Plasmas **13**,112701 (2006).
[15] C. K. Li *et al.*, Phys. Rev. Lett. **97**, 135003 (2006).
[16] M. M. Marinak *et al.*, Phys. Plasmas **5**, 2275 (2001).
[17] J. M. Soures, *et al.*, Phys. of Plasmas **3**, 2108 (1996).
[18] F. H. Séguin *et al.*, Rev. Sci. Instrum. **74**, 975 (2003).
[19] D. D. Meyerhofer *et al.*, Phys. Plasmas **8**, 2251 (2001).
[20] J. R. Rygg *et al.*, Science **319**, 1223 (2008).
[21] C. K. Li *et al.*, Phys. Rev. Lett. **100**, 225001 (2008).
[22] G. B. Zimmerman and W. L. Kruer, Comm. in Plas. Phys. and Contr. Fus. **2**, 51 (1975).
[23] C. K. Li *et al.*, Phys. Plasmas **7**, 2578 (2000).
[24] An asterisk structure similar in character to that described herein were observed, though not explicitly nor quantitatively discussed, from Au plasma x-ray self-emission in Nova 5-beam drive hohlraum experiments. S. H. Glenzer *et al.*, Phys. of Plasmas **6**, 2117 (1999).
[25] For 3.3 (15) MeV protons, the energy loss from passing through 1 mg cm^{-2} of Au plasma is ~ 100 (20) keV. Though negligible, scattering effects, as shown for the Au-plasma at hand, are in fact consequential.
[26] V. L. Highland, Nucl. Instrum. Methods **129**, 497(1975).
[27] Though we feel this scenario is unlikely, we cannot experimentally exclude the possibility that the proton depletion region of the asterisk structure is a result of intense, local *E* fields associated with strong azimuthally -oriented pressure gradients of the jet-Au plasma.
[28] With the separation between the electrons and ions on the order of a Debye length (λ_D), and an ion inertial response on the order of an ion plasma frequency (ω_{pi}), a representative speed is obtained: $C_s = \lambda_D \omega_{pi}$.